Dimer-parity-dependent odd-even effects in photoinduced transitions to cholesteric and twist grain boundary smectic-C^* mesophases: Experiments and simulations

Rajalaxmi Sahoo,[1,2] Dibyendu Maity,[3] D. S. Shankar Rao,[1,*] Suman Chakrabarty,[3,†] C. V. Yelamaggad,[1] and S. Krishna Prasad[1]

[1]*Centre for Nano and Soft Matter Sciences, Shivanapura 562162, India*
[2]*Manipal Academy of Higher Education (MAHE), Manipal 576104, India*
[3]*Department of Chemical and Biological Sciences, S. N. Bose National Centre for Basic Sciences, Salt Lake, Kolkata 700106, India*

(Received 21 June 2022; accepted 16 September 2022; published 17 October 2022)

We describe investigations on the influence of the flexible spacer parity and length of the guest photoactive liquid-crystalline dimers in guest-host mixtures exhibiting photoinduced transitions involving isotropic (I), cholesteric (N^*), and twist grain boundary smectic-C^* (TGBC^*) phases. Despite a small concentration (3 wt. %) of the guest molecules, the transition temperatures and their photodriven shift (δT) show a strong odd-even parity (of the dimer) dependent effect, with the even-parity systems having a larger value than their odd-parity counterparts; δT is larger for the N^*-TGBC^* transition than for the I-N^* one. The photocalorimetric measurements corroborate these features in addition to showing that, in comparison with the absence-of-ultraviolet (UV) case, the transition enthalpy (ΔH) of the I-N^* transition in the UV-on case is diminished by 33 and 12% for the mixtures with even- and odd-parity dimers, respectively. The duration for relaxation from the isothermal photodriven transition also exhibits general features of an odd-even influence. Molecular dynamics simulations demonstrate the presence of significant conformational heterogeneity and associated shift in the conformational space on photostimulation of the guest molecules. The change in the effective shape and nematic order parameter is more pronounced in the even-parity system.

DOI: 10.1103/PhysRevE.106.044702

I. INTRODUCTION

Frustrated structures arising from a competition between two different types of ordering are ubiquitous in liquid crystals (LCs). The competition could be in length scales as in smectic phases, between helical structures and topological constraints in blue phases (BPs), and between chirality of the molecules and the demand to form layered structures in twist grain boundary (TGB) phases [1–7]. The last two of these have close association with the cholesteric (N^*) phase, which is actually an orientationally ordered fluid but with a superimposed helical order owing to the presence of chiral molecules; the helical axis is normal to the director (orientation direction of the molecules) [8,9]. The TGB phase, forming the topic of this paper, has especially drawn interest since it adds another element to complete the analogy between LCs and superconductors [10,11]. The presence of the chiral molecules superimposes a helical twist on the layered structures. However, because of the necessity to retain their identity, the smectic forms blocks which in turn rotate in a helical fashion, thus satisfying chirality as well as stratification aspects [12,13]. In fact, as is true in many other aspects, the LCs expand the scope of such structures by having three different TGB phases, viz., TGB-A, TGBC, and TGBC^*, the last letter in each case indicating the nature of the smectic phase that forms the blocks: A for smectic-A having molecules along the layer normal and C and C^* for molecules forming an angle with respect to the layer normal [14–21]. It must be added that, in the TGB-A and TGBC phases, the only helicity is N^*-like, while in the TGBC^* phase, the smectic ordering also has a helical structure of its own (along the layer normal) in addition to the N^*-like helix, with the two helices being in orthogonal directions. We have been working on influences of dopants on the structure and properties of the TGBC^* phase and, for example, demonstrated [22] that, even at dilute concentrations, the added gold nanorods of a small aspect ratio can substantially increase the thermal range of the TGBC^* phase. Other interesting observations have been that the wavelength-corresponding pitch of the N^*-like helix exhibits a redshift or blueshift depending on the concentration of the nanoinclusions, the width of this photonic bandgap (PBG) and the smectic layer thickness also increase, and the spacing of the square grid pattern, a hallmark of the TGBC^* phase, more than doubles. It is known that presence of certain dye molecules, especially of the azobenzene derivative types [7,23–33], in a smectic structure and the system subjected to photoisomerization can lead to the feature of nanophase segregation [34–36]. With this background, using an azo-derivative-tailored actinic light, we investigated the influence of photoisomerization on the properties of the TGBC* phase [37]. The photoisomerization of an azobenzene molecule involves photodriving its equilibrium low-energy E (*trans*) conformer to the high-energy Z (*cis*)

*raoshankards@gmail.com
†sumanc@bose.res.in

conformer. Upon turning the illumination off, the *Z* conformer would revert to the *E* conformer through a process known as the thermal back relaxation (TBR). At least in a monomeric azobenzene molecule, the *E* conformer has essentially a rod shape, while the *Z* conformer is significantly bent. The actinic light brought about several attractive changes to the system, including intensity-dependent transition temperature, large blueshift of the PBG wavelength, and significant variation of the spacing of the square grid, all of which exhibit fast dynamics between the equilibrium and photostationary states. The phenomenon of nanophase segregation was also proposed [34–36], wherein the spatial placement of the azobenzene derivatives will depend on whether they are in their equilibrium *E* or photodriven *Z* conformations.

At this point, it is relevant to recall that the photoisomerization-related influences can be expected and indeed observed to be more if one replaces the monomeric azobenzene derivative traditionally used for such experiments with a mesogenic dimer [38–40] that contains an azobenzene moiety in both its arms. In an earlier work, we [41] showed that, in dimers wherein the two mesogenic monomers are linked by an alkylene flexible spacer, the parity and the length of the spacer play an important role in controlling the thermal stability of the nematic phase vis-à-vis its transition to the isotropic phase. Prompted by these studies, in this paper, we have experimentally investigated the influence of azobenzene dimers on the transition temperature, dynamics of the photodriven and TBR processes, and photocalorimetric parameters across the isotropic liquid (*I*)-*N** and *N**-TGB*C** transformations in a guest-host LC system comprising a nonphotoactive host. Preliminary molecular dynamics (MD) simulations have also been carried out to illustrate the complexity of the problem that these systems involve a multitude of conformations, their populations, and nontrivial changes between the equilibrium and photostationary states. Some salient features of the experiments and the simulations are (i) in contrast to their odd-parity counterparts, the even-parity dimers exhibit a larger shift in the transition temperatures of both *I*-*N** and *N**-TGB*C**, with the latter an order of magnitude larger, (ii) the dynamics of the photodriven isothermal transformation, especially the light-off one, shows an odd-even effect for the *I*-*N** transition but not for that involving the TGB*C** phase. However, unlike the former transition, the *N**-TGB*C** transformation has comparable timescales (∼10–50 s), (iii) MD simulations demonstrate the presence of significant conformational heterogeneity in the host and guest molecules due to the flexible linker region, and photostimulation of dopants leads to a significant shift in the conformational population. The change in the effective shape of the dopants is the primary reason behind the shift in the transition temperature. The variations in the characteristics of the conformational ensemble and in the nematic order parameter (NOP) are more pronounced for the even parity, a feature consistent with the experimental results.

II. MATERIALS AND METHODS

A. Experimental

Ternary mixtures comprising a nonphotoactive host and a photoactive guest, both of which are liquid crystalline, were

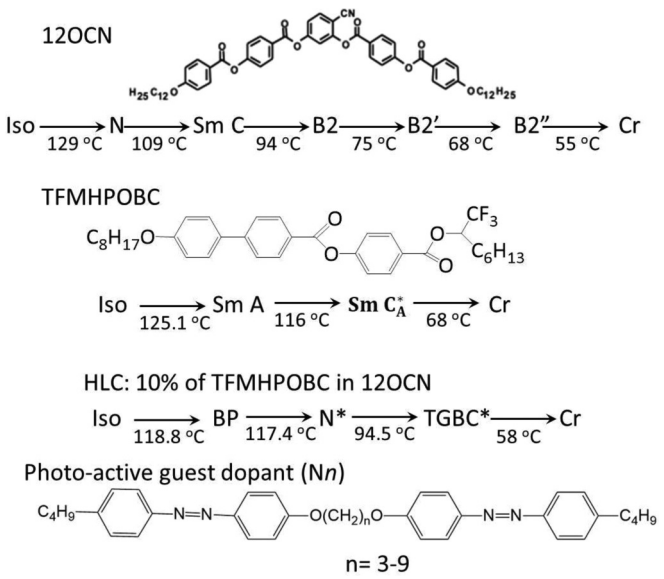

FIG. 1. Molecular structures of the guest photoactive azo dimer (N*n*) and the host liquid crystal (HLC) mixtures. The phase sequence and the transition temperatures for HLC are also provided. In the final mixtures, referred to as M*n* ($n = 3$–9, *n* being the number of methylene units in the central linkage), the azo dimer and HLC are present in the ratio of 3:97, by wt. %.

employed for the study. The host LC (HLC for short) material, a binary mixture of a chiral rodlike material (TFMHPOBC) [42] and a bent core compound (labeled 12OCN) [43], contained in the ratio of 9:1, exhibits *I*-BP-*N**-TGB*C** phase sequence. The guest component is a photoactive dimeric azo material (N*n* for short) with a central flexible spacer having methylene units whose value varies from $n = 3$ to 9 and exhibiting the nematic mesophase [44]. While TFMHPOBC was procured from Showa Shell Inc., 12OCN as well as the azo dimers were synthesized in our labs. The molecular structure of the constituents along with the transition temperature for HLC are mentioned in Fig. 1; the transition temperatures of the photoactive dimers as a function of spacer length (*n*) are shown Fig. S1 in the Supplemental Material [45]. The point to be noted about the dimers is that the two azo groups are symmetrically disposed about the central methyl spacer, a feature expected to enhance the photoisomerization effect. The employed ternary mixtures consisted of 3 wt. % of N*n* in HLC and are hereafter referred to as M*n* ($n = 3$–9). Most of the experiments described in this paper were conducted on 8-μm-thick samples sandwiched between two glass plates whose inner sides were pretreated with a polymer layer (PI2555, Merck) and rubbed unidirectionally for planar alignment of the LC molecules. In this configuration, the helical axis in the cholesteric phase will be normal to the substrate. The uniformity, phase sequence, and the transition temperature of mixtures were determined by texture observations of the sample under a polarizing microscope (POM; Leitz DMRXP, Weinheim, Germany). Figures 2(a) and 2(b) show the POM photographs with planar alignment of the molecules in the *N** and TGB*C** phases, respectively, for the representative material M4. The *N** and TGB*C** phases are identified from the oily streak texture and grid pattern with the simultaneous existence of Grandjean cano lines in a wedge cell, respectively.

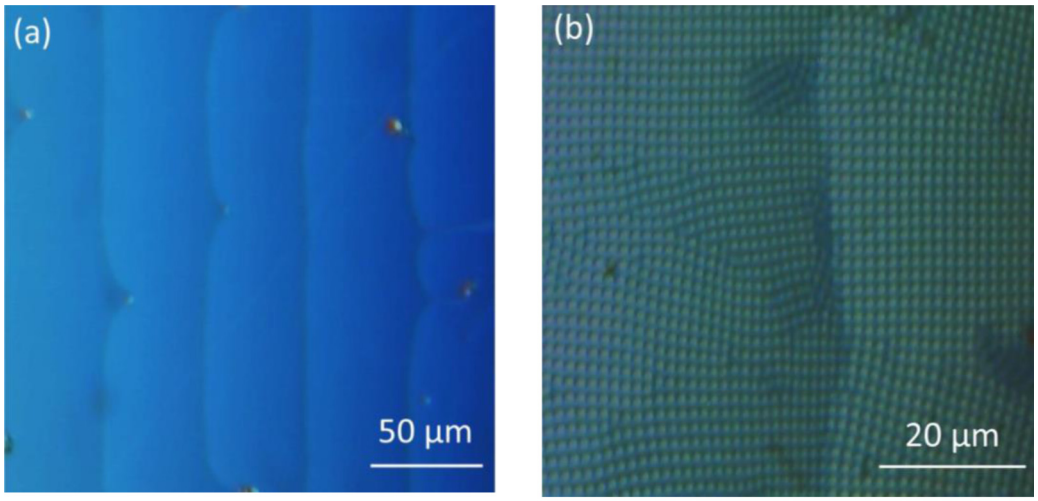

FIG. 2. Representative polarizing microscope (POM) photographs (for M4 sample) showing planar aligned texture in the (a) N^* and (b) twist grain boundary smectic-C^* (TGBC^*) phase. Whereas N^* shows only Grandjean cano lines, the TGBC^* phase has a superimposed square grid pattern also.

The photoisomerization experiments were conducted by illuminating the sample with the ultraviolet (UV) beam obtained from an intensity stabilized UV source (Hamamatsu LC5, L8333-01, Japan) equipped with a fiber-optic guide. A narrow bandwidth UV-pass visible cut filter (UG-11, Newport, UK) with a peak wavelength of 365 nm was inserted in the UV beam path. An additional infrared (IR)-block filter was introduced between the sample and the UV source to prevent undesirable sample heating. The intensity of the UV radiation (I_{UV}) falling on the sample after passing through the filter combination was measured using a UV power meter (Hamamatsu, C6080-03, Japan) placed in the sample position. The phase transition was monitored by collecting thermal variation of the laser intensity (I_{laser}) transmitted through the sample by a photodiode; the schematic of the apparatus is shown in Fig. S2 in the Supplemental Material [45].

Photocalorimetric measurements were made using a commercial differential scanning calorimeter (DSC; Model 8000, Perkin-Elmer, USA) after making modifications to enable simultaneous irradiation of both the sample and the reference cups; the schematic of the apparatus is shown in Fig. S3 in the Supplemental Material [45]. The intensity stabilized UV source mentioned above was used. However, instead of the typical single output fiber-optic cable, we used a two-way split cable that had the capability to split the incoming beam from the source into two equal halves and feeding them into two secondary fiber-optic cables. Each of these cable terminations was positioned normal to the DSC sample chamber to UV irradiate the sample and the reference cups. The entire chamber was maintained in an inert atmosphere by passing nitrogen gas and covered with glass, polytetrafluoroethylene, and Styrofoam sheets for good thermal insulation. The actual intensity of the UV light illuminating the sample was determined using a UV power meter (Hamamatsu, C6080-03, Japan).

B. Computational studies

Atomistic classical MD simulations were performed using GROMACS software (ver. 2019.5) [46]. We used the GROMOS force field using ATB Web server [47] to model both HLC and guest molecules (N3T, N3C, N4T, and N4C; T stands for *trans* or *E* conformations and C stands for *cis* or *Z* conformations). Each system consisted of 10 guest molecules randomly inserted into 200 HLC molecules. All systems were energy minimized using steepest descent method followed by two-step equilibration in NVT and NPT ensembles. Due to its sluggish dynamics, the system was further equilibrated using a simulated annealing protocol in the NPT ensemble, where the system was gradually heated to 600 K (to ensure rapid mixing and rearrangement of constituent molecules within the simulation timescale) followed by gradual cooling to the target temperature 343 K over the duration of 50 ns. During the production run, the temperature was maintained at 343 K using the velocity rescale method [48] with a relaxation time of 1 ps, and the pressure was kept constant at 1 atm using a Parinello-Rahman barostat [49]. All simulations were performed using periodic boundary conditions in all directions, and the long-range interactions were calculated using the particle mesh Ewald summation method. The cutoff distance for electrostatic and van der Waals interactions was set to 1.0 nm. The hydrogen-containing bonds were constrained with LINCS, and the integration time step was set to 1 fs. All production runs were performed for 200 ns with the trajectory being saved every 10 ps. Visualization of molecular structures was performed using VMD [50].

III. RESULTS

A. Effect of photoisomerization on the transition temperatures

The mixtures M*n* exhibit the same phase sequence as exists for HLC except for the disappearance of the BP. This may not be surprising and can be attributed to the reduction of the chiral influence as N*n* are achiral compounds. It is to be noted that the clearing point, the temperature at which the material transforms from the isotropic phase, is hardly altered in contrast to the N^*-TGBC^* transition. These features suggest subtle changes in the chiral character of the medium

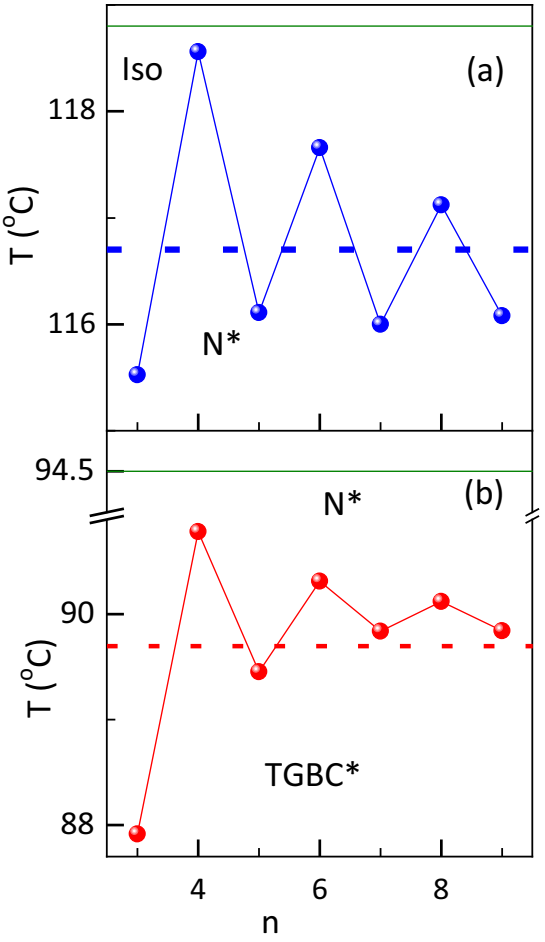

FIG. 3. Spacer length (n) dependence of the (a) I-N^* and (b) N^*-twist grain boundary smectic-C^* (TGBC^*) transition temperatures obtained without ultraviolet (UV) illumination for the mixtures M3–M9, exhibiting a strong odd-even effect. The blue and red solid lines serve as guides to the eye. The dashed lines represent the mean value of the respective transition temperatures taking the average of the values for all mixtures M3–M9. For comparison, the transition temperatures for host liquid crystal (HLC) are shown as green solid lines.

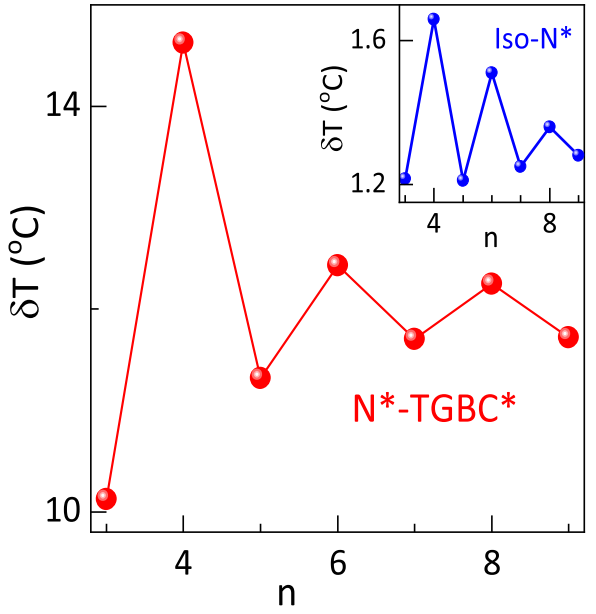

FIG. 4. Photoinduced shift in the transition temperature δT [$= (T_{nUV} - T_{UV})$, T_{nUV} and T_{UV} being the transition temperature without and with ultraviolet (UV) radiation] for the N^*-twist grain boundary smectic-C^* (TGBC^*) transition as a function of spacer length (n). Inset shows the same parameter for the I-N^* transition. Clearly, mixtures with even-parity dimers have a larger δT than the mixtures with odd-parity dimers, the effect being stronger for the N^*-TGBC^* transition.

influencing the BP and TGBC^* phases more than the N^* phase.

Figure 3 presents the transition temperatures of the I-N^* and N^*-TGBC^* transformations for the different Mn mixtures. A remarkable odd-even effect is seen in both cases even though the material causing the alternation, the Nn compounds, is present at a low dilute concentration of 3 wt. %. As may be expected, the mixtures with even-parity Nn dopant exhibit a higher transition temperature than the odd-parity ones, resulting in an alternation in the value as n increases. While the strength of alternation is comparable for the two transitions at the lowest values of $n(=3, 4)$, it rapidly diminishes with increasing n for the N^*-TGBC^* transition. The difference in the behavior of the two transitions can be better seen by calculating the mean value of the transition temperature over the entire range of $n = 3$–9 studied (see Fig. 3). A final point that we would like to make in this regard is that the alternation which is a hallmark of symmetric dimers is seen even at a low concentration, suggesting that the contribution of the dimers is retained to a large extent even in the ternary mixtures. With this background, let us look at the influence of photoisomerization.

The photoinduced shift in the transition temperature [$\delta T = (T_{nUV} - T_{UV})$, T_{nUV} and T_{UV} being the transition temperatures without and with UV radiation] for the N^*-TGBC^* transition as a function of n is shown in Fig. 4. It should be reiterated that the employed UV intensity is very low (1 mW/cm^2) in addition to the fact that there is an IR filter between the UV source and the sample. Thus, the radiation-driven heating may be negligibly small, and the observed photoinduced finite δT is essentially due to the change in the conformation of the guest azo molecules. Similar data obtained for the I-N^* transition are shown in the inset of Fig. 4. It is evident from the figure that δT for the N^*-TGBC^* transition is higher than that for the I-N^* transition. More interestingly, there is a pronounced odd-even effect for δT as a function of n. For example, for the M4 material, δT values are 14.6 and 1.7 °C for the N^*-TGBC^* and I-N^* transitions, respectively, while for the M3 mixture, they are 10.1 and 1.2 °C for the N^*-TGBC^* and I-N^* transitions, respectively. The feature that δT is more for the transition involving the TGBC^* phase agrees with our previous work having a monomeric azobenzene compound as the photoactive guest [37]. Let us now compare the δT values for situations wherein another mesophase transition apart from I-N is also studied. Reporting measurements on a few chiral LCs, Joly *et al.* [51] found that the δT values were higher or not for a transition other than the I-N (here, we do not differentiate between the achiral N or its chiral

equivalent N^* phase) dependent on the phase sequence itself. When the phase present immediately below N was the TGB phase [51], δT was smaller for the I-N than for N-TGB. The situation was opposite when the N phase directly transformed to the Sm-C^* phase. In another case [35] wherein the N phase directly transformed to the Sm-A phase, the δT value was nearly an order of magnitude smaller for the N-Sm-A than for the I-N. Like the finding of Joly *et al.* [51], Prasad *et al.* [52] found that, when another phase supporting a twisted supramolecular arrangement (twist-bend nematic or N_{TB}) but not having a proper layered structure is present immediately below the N phase, δT is relatively smaller for the I-N transition than the second transition. Since both TGB and N_{TB} could arise due to factors that compete to coexist with the twisted architecture, a larger δT for transitions involving those phases can be associated with the underlying frustration. It is possible that the photoinduced Z isomers have less favor for these frustrated structures than for the simply orientationally ordered cholesteric mesophase. A point that should still be borne in mind is that, in the present case as well as those in Refs. [35] and [52], the photoactive material forms a minority component unlike the other situation cited above [51]. It is also interesting to note that the T values for the N^*-TGBC^* transition are more in the present system having dimer photoactive molecules (with two azo entities per molecule) than in the previously reported case of a monomeric azobenzene derivative as the dopant [37]. Surprisingly, the photoinduced effect for I-N^* phase is essentially the same for the monomeric and dimeric cases, perhaps indicating that the presence of two azo groups has more influence on the transition involving the frustrated phase.

Summarizing this section, a salient feature observed is that, despite the small concentration (3 wt. %) of the dopant and the small UV power (1 mW/cm^2), there is a strong spacer-parity/length-dependent, odd-even effect in the δT value for the N^*-TGBC^* transition for all the Mn mixtures investigated. This feature is found to be true for the I-N^* transition also, albeit the value is nearly an order of magnitude smaller. Additionally, just like the transition temperature ($T_{I\text{-}N^*}$ and $T_{N^*\text{-TGB}C^*}$), the magnitude of the alternation in δT value decreases with increase in n with the extent of decrease being stronger for the N^*-TGBC^* transition than for the I-N^* one. A notable behavior that has been observed is that, if the HLC used here is substituted by a LC having molecules with a strong dipole along their long molecular axes, the δT values are much larger for the I-N^* transition. Additionally, even lower UV intensities could bring larger effects, suggesting that the polarity of the host molecule also plays an important role in deciding the magnitude of δT.

B. DSC

We have performed calorimetric measurements on two representative mixtures M5 and M6. To ensure that there are no significant UV depletion effects, the sample had to be kept thin. This required using a very small quantity of the sample (200 μg) which resulted in low thermal response and perhaps was responsible for the hardly discernable thermal signature for the N^*-TGBC^* transition, notwithstanding the fact that this transition has a second-order character. In fact, having a high scanning rate (10 °C/min) also did not help in obtaining any signature of the transition. Hence, we discuss the influence of photoisomerization on the I-N^* transition only. Figures 5(a) and 5(b) show the DSC scans across the I-N^* transition for M5 and M6 in the absence of and with UV radiation ($I_{\mathrm{UV}} = 0.8$ mW/cm^2). Photoisomerization decreases the peak temperature (taken to be $T_{I\text{-}N^*}$), broadens the profile, and notably the area under the peak, a measure of the associated enthalpy (ΔH). As we shall see below, the photo effect is more for the mixture with the even azo dimer (M6). To extract the peak parameters, we fitted the profiles to a Gaussian expression. The best-fit parameters of $T_{I\text{-}N^*}$, full width at half maximum (FWHM), ΔH, and the two parameters which

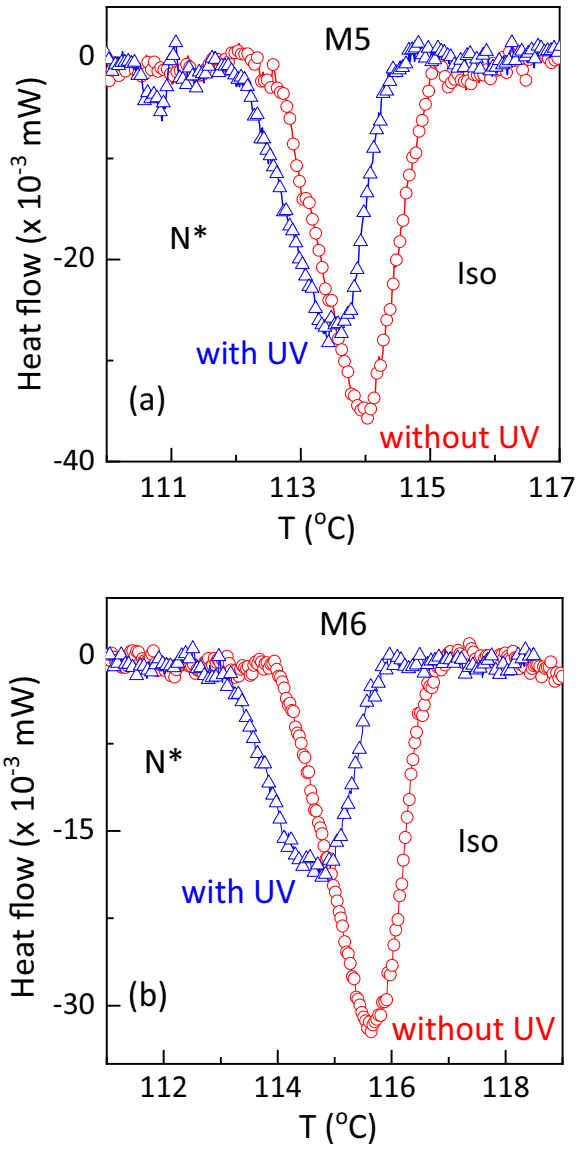

FIG. 5. Differential scanning calorimetric scans for (a) M5 and (b) M6 mixtures (having the odd-parity N5 and even-parity N6 dimers, respectively) across the I-N^* transition without (red) and with ultraviolet (UV) illumination of $I_{\mathrm{UV}} = 0.8$ mW/cm^2 (blue). Both the peak temperature (taken to be $T_{I\text{-}N^*}$) and the transition enthalpy (ΔH) reduce upon UV illumination, the effect being more for the even-parity dimer case than for the odd one.

TABLE I. Parameters from the calorimetric scans obtained with and without UV for M5 and M6 mixtures.

	M5		M6	
	Without UV	With UV	Without UV	With UV
$T_{I\text{-}N^*}$ (°C)	114.02	113.4	115.7	114.8
Width (K)	1.29	1.29	1.38	1.53
ΔH (J/g)	1.33	1.17	1.5	1
δT (°C)		0.62		0.9
$\delta\Delta H$ (J/g)		0.16		0.5

highlight the photo effect, viz., δT and $\delta\Delta H$, the difference in the values without and with UV radiation, are shown in Table I. The magnitude of δT as well as $T_{I\text{-}N^*}$ agree with the data from the laser transmission experiment and emphasize the fact that the even dimer mixture (M6) has a larger (0.9 °C) shift in the photoinduced transition temperature. Interestingly, the width of the transition (FWHM) is hardly changed by UV illumination in the case of M5 (1.29 K) but substantially increased (by 10%) for the M6 system. A similar effect is seen for the transition enthalpy: $\delta\Delta H(=\Delta H_{\mathrm{nUV}}-\Delta H_{\mathrm{UV}})$, the photoinduced change in ΔH is higher for M6 (33%) than for M5 (12%). In fact, the associated entropy change shows similar variation with $\delta\Delta S$ values being 13 and 33% for M5 and M6, respectively. It must however be emphasized that the change in entropy/enthalpy is brought about by the odd-even parity change of the azo dimer, which is present at a low concentration of 3 wt. %. The difference in the transition entropy (ΔS) between the even and odd dimers (M5 and M6) under no UV conditions is found to be 0.45 mJ/gK for the thermal transition. In the light of this, it is interesting to note that $\delta\Delta S$ for M6 is higher by a value of 0.88 mJ/gK than for M5. The photodriven value being higher than the thermal one thus suggests that, at the molecular level, the conformational changes across the transition are drastically more for the photodriven case than for the thermal case.

C. Dynamics of the photoinduced phase transitions

As already discussed in the Introduction section, the E isomer of the photoactive dopant, being the low-energy form, is the equilibrium structure, and the Z isomer obtained by photoisomerization is an unstable one. Thus, once created, the Z form will return to the initial equilibrium state (E form), either spontaneously through the TBR or stimulated by shining white (or specifically blue) light. Since the photoactive molecules are the minority component, the dynamics of both the forward (photodriven) and the backward (TBR) processes are significantly influenced by the nature of the phases involved and the type of the host molecules. Further, the odd-even parity of the dimer, seen to influence the δT values, can also be expected to have a bearing on the dynamics of these processes. With these features in the background, we carried out time-dependent studies by monitoring I_{laser} as a function of time while the UV light was turned on and subsequently off with the sample held at a particular temperature.

The raw temporal profiles of I_{laser} in the N^* and TGBC^* phases of the mixture M4 are shown in Fig. 6. The scans

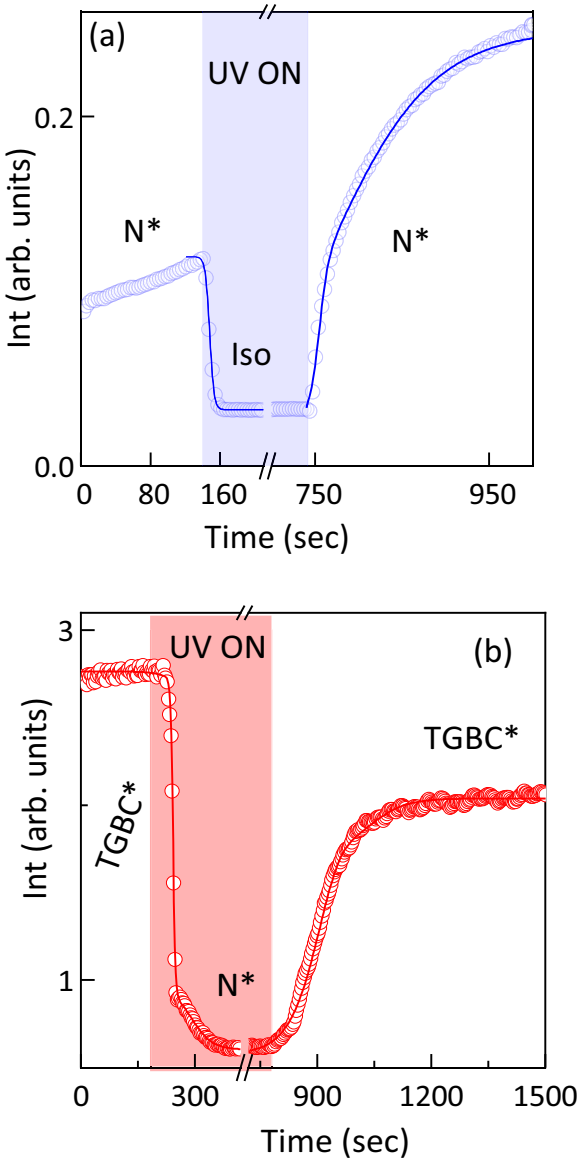

FIG. 6. Temporal variation of I_{laser} of the M4 mixture when the ultraviolet (UV) illumination ($I_{\mathrm{UV}}=1$ mW/cm^2) is turned on for the duration indicated by the colored box and subsequently off while the sample was held at a constant reduced temperature of (a) $T_{\mathrm{red}\,1}=1$ °C ($T_{\mathrm{red}\,1}=T_{I\text{-}N^*}-T$) in N^* and (b) $T_{\mathrm{red}\,2}=5$ °C ($T_{\mathrm{red}\,2}=T_{N^*\text{-TGB}C^*}-T$) in the twist grain boundary smectic-C^* (TGBC^*) phase. The solid lines in the panel represent the fitting to Eq. (1).

were collected at $T_{\mathrm{red}\,1}=1$ °C ($T_{\mathrm{red}\,1}=T_{I\text{-}N^*}-T$) [Fig. 6(a)] and $T_{\mathrm{red}\,2}=5$ °C ($T_{\mathrm{red}\,2}=T_{N^*\text{-TGB}C^*}-T$) [Fig. 6(b)]. For the clearing temperature (N^*-I transition), the UV-on process is faster than the relaxation process, while a trend reversal is observed for the TGBC^*-N^* transition. In the case of the photodriven N^*-I transition, the I_{laser} variation is through a single steplike change, whereas the off process seems to comprise two time constants while the opposite is true for the TGBC^*-N^* transition. To quantitatively extract the associated response times, τ_{on} and τ_{off}, we fitted the data to a

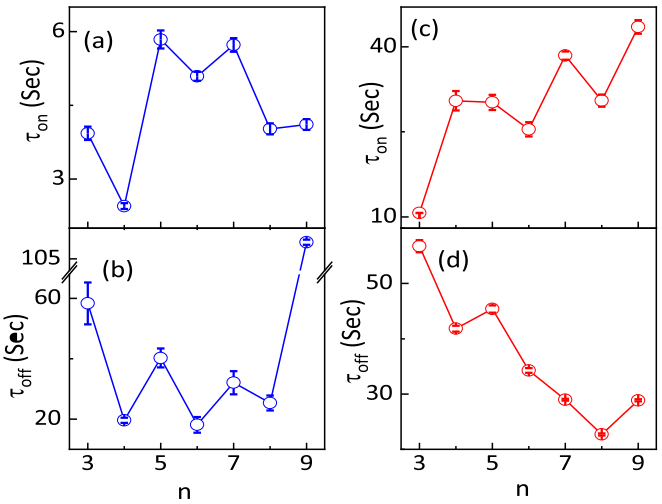

FIG. 7. Spacer length (n) dependence of the durations for the ultraviolet (UV)-on (τ_{on}) and UV-off (τ_{off}) processes at a reduced temperature of (a) and (b) $T_{red1} = 1$ °C in the N^* phase and (c) and (d) $T_{red\,2} = 5$ °C in the twist grain boundary smectic-C^* (TGBC^*) phase.

single/double sigmoid function:

$$I(t) = I_0 + I_1\left\{1 + \exp\left[\frac{(t_c - t)}{\tau_{sig}}\right]\right\}^{-1}. \quad (1)$$

Here, I_0 is the baseline, I_1 is the amplitude, t_c is the instant at which the response reaches the midpoint, and τ_{sig} are the characteristic response times. The spacer length (n)-dependent τ_{on} and τ_{off} data obtained from such a fitting for the I-N^* transition are presented in Figs. 7(a) and 7(b) (for the cases where the double sigmoid was used, the τ values given are the sum of the values obtained from the two functions). As would be obvious even from the profile shown in Fig. 6(a), the τ_{off} values are about an order of magnitude larger than the τ_{on} values. More importantly, a clear odd-even effect is observed in the τ_{off} data, although an exceptionally high value is seen for the M9 material. However, given the error in the measurement (1.5 s), no definitive conclusion could be drawn about the behavior of τ_{on} with the spacer length. In contrast, for the N^*-TGBC^* transition [Figs. 7(c) and 7(d)], although the values are not strictly monotonic, there is a clear increasing (for τ_{on}) and decreasing (for τ_{off}) trend seen when the spacer length is increased. It must also be pointed out that, for the lowest spacer length material (M3), τ_{off} is higher (factor of 5) than τ_{on}, whereas for M9, it is the opposite.

It should be recalled here that the photoinduced shift in the transition temperature (δT) is larger for even-spacer-length systems than for odd-spacer ones (Fig. 4). Upon UV illumination in the N^* phase at a particular reduced temperature ($T_{red\,1} = 1$ °C; $T_{red\,1} = T_{I\text{-}N^*} - T$), the sample is driven deep into the isotropic phase for the odd-spacer case than the even-spacer one. This will result in, as shown in Fig. 7(b), τ_{off} being higher for the odd-spacer ones. The twin-relaxation feature seen in the TBR process for the I-N^* transition seems to be a general behavior since systems with a monomeric azobenzene derivative as a photoactive dopant [37] also show it. An interesting feature is that, despite being at comparable temperatures, the τ_{off} value observed here is faster (by a factor of 4) than in our previous studies [37] which employed a monomeric azobenzene derivative, pointing to the fact that the photodriven conformational change in the azo dimers is more strained than in the monomeric one.

1. Influence of the magnitude of I_{UV} *on the dynamics*

For all mixtures M3–M6, the raw profile of I_{laser} vs time for the TGBC^*-N^* transition appear quite like that for M4, as shown in Fig. 6(b). However, when the spacer length is further increased, a subtle but clearly noticeable feature starts appearing on turning the UV on: a small peaklike trait precedes the steplike fall. Additionally, the details of this overshoot are seen to be clearly dependent on the magnitude of I_{UV} employed, as shown in Figs. S4(a) and S4(b) in the Supplemental Material [45] for the M7 mixture. It must be remarked that this overshoot is not present for M3–M6 but appears for M7–M9, having maximum strength for M7. To describe the profiles, we fitted the data during the UV-on process to a double sigmoid function, and an exemplary case of the data for $I_{UV} = 0.8$ mW/cm^2 is shown in Fig. S4(c) in the Supplemental Material [45]. As expected with increasing I_{UV}, the rate for the sigmoid function describing the overshoot rapidly diminishes to a vanishingly small number. The rate for the main steplike fall also decreases but far more slowly. The overall time taken as the combined rates of the two sigmoids falls as an exponential variation with I_{UV}, as seen in Fig. S4(d) in the Supplemental Material [45]. Efforts to associate these features with spectroscopic data providing information about the population of E and Z conformers are underway. Notwithstanding this attempt, it is clear from the simulation studies, to be described below, that the conformations adapted by these dimers are much more complex.

D. Simulation studies

We have used classical atomistic MD simulations to establish a microscopic picture of the conformational ensemble of the host-guest mixture and their packing efficiency that is likely to be an important factor controlling the transition temperatures. Figure 8(a) shows a representative snapshot of the simulation box (with periodic boundary conditions). The photoactive guest molecules are dispersed in the background of HLC molecules. Figure 8(b) focuses on the nearest neighbors of a particular guest molecule (N4T). Given the nonlinear or bent conformations of both the host and guest molecules, a perfectly parallel stacking or alignment would not be possible or optimal. Instead, two different strands/arms of these molecules have locally parallel packing (orientational ordering), as clearly visible in Fig. 8(b). Two different arms of the molecules may exist in different orientations created by rotation around the flexible linker region. Thus, the overall packing efficiency would strongly depend on the conformational heterogeneity of the host and guest molecules. Clearly, the nematic or smecticlike ordering in this system cannot be described by simplified rigid rodlike or ellipsoidal models, as routinely done to describe liquid crystalline systems [53].

As discussed above, to understand how the different conformers of the photoactive guest molecules locally perturb the

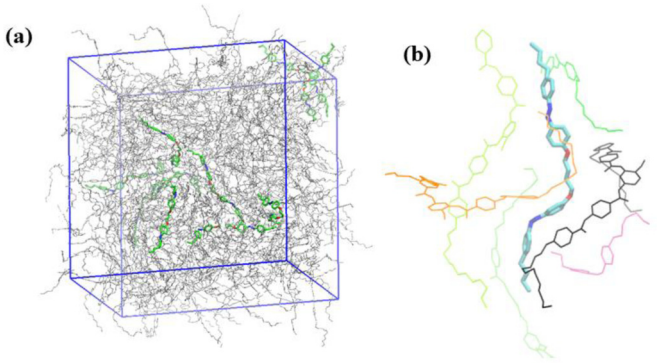

FIG. 8. (a) A representative snapshot of the simulation box. The guest N3T (T indicates *trans* or *E* conformation) and host liquid crystal (HLC) molecules are shown in color and in gray tint, respectively. (b) Packing arrangement of the HLC molecules around a representative N4T guest molecule (having the evident azo linkage shown in blue).

packing and orientational ordering of the host molecules, it is crucial to investigate the conformational space explored by the guest molecules N3 and N4 in their respective ground states (N3T, N4T) and photoexcited states (N3C, N4C). We expect that, in the ground state *trans* configurations (N3T, N4T), the guest molecules would adopt a linear shape, whereas the photoactivated *cis* configurations (N3C, N4C) would involve a bent shape that is likely to disturb the local orientational ordering of the HLC molecules. However, our MD simulations indicate that, given the conformational flexibility of the linker region connecting the photoactive dimers, there exists a considerable conformational heterogeneity for both the *trans* and *cis* conformations, leading to a large variation in the possible structures. We have characterized the conformational space sampled by the guest molecules using the joint probability density (histogram) of two geometric/structural parameters: (i) the angle between the two arms of the guest dimer molecules and (ii) the end-to-end distance between the outermost atoms of the last two aromatic rings (Fig. 9). The geometric definitions of these parameters for the N3 and N4 guest molecules have been clarified in Fig. S5 in the Supplemental Material [45].

We observe that there are multiple metastable states in the conformational space of the guest molecules rather than a unique conformation. Thus, the guest molecules do not have a specific rigid shape. Rather, due to the flexibility of the linker region, the two arms of the dimer can have multiple distinct orientations leading to the observed different configurations/shapes. A few representative configurations from the major peaks of the probability distributions are also shown in Fig. 9 to highlight the conformational heterogeneity.

Interestingly, even for the *trans* conformations of the N = N bonds, it is possible for the molecule to exist in a bent or U-like conformation with a low end-to-end distance, as observed for the N4T system. The photoactivation (*trans* to *cis* transition) leads to a large shift in the conformational ensemble both in terms of the hinge angle and the end-to-end distance. It seems that the end-to-end distance distribution shifts to larger values for N4, whereas it decreases slightly for the N3. Moreover, the overall changes in the effective shape

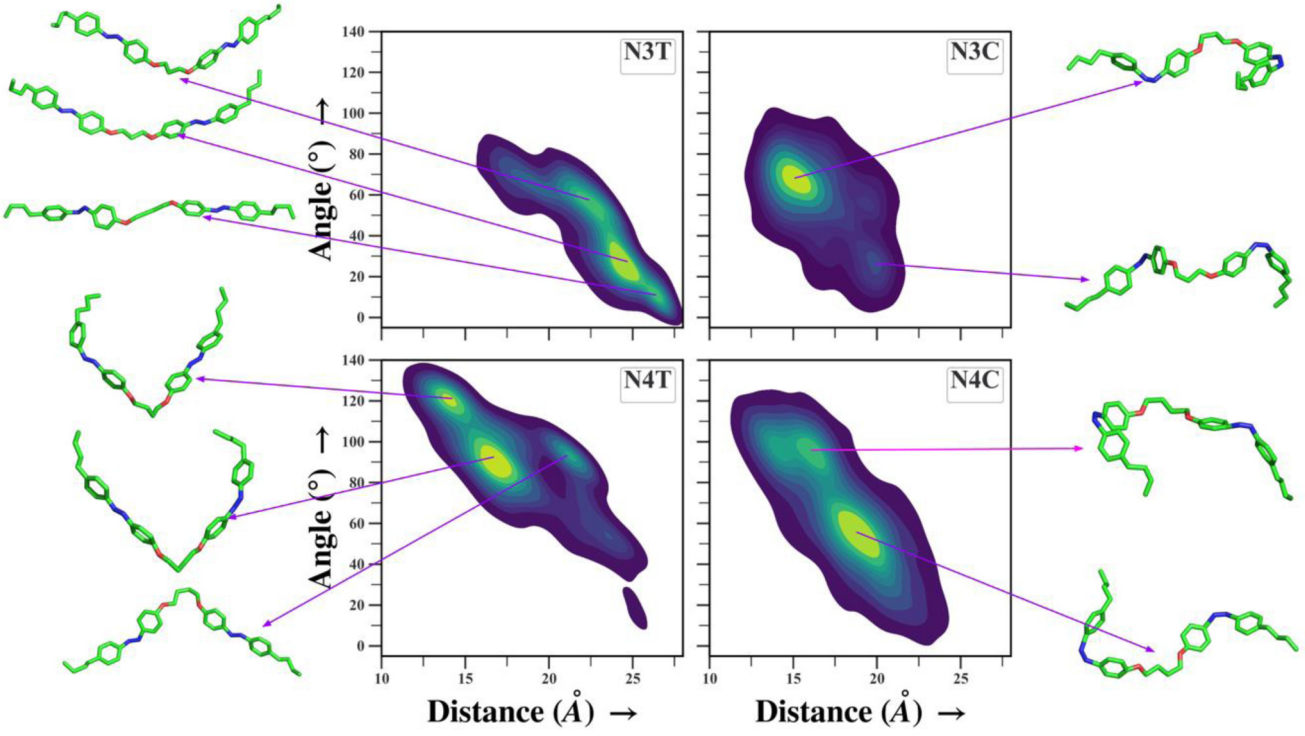

FIG. 9. Joint probability density (histogram) of the angle between the two arms of the guest dimer molecules (*y* axis) and end-to-end distance (*x* axis) for the two guest dimer molecules in their *trans* (*E*) and *cis* (*Z*) conformations. Representative molecular structures from the most probable regions are shown as well to highlight the conformational heterogeneity of the guest molecules.

of the guest molecules seem to be more pronounced in the case of even-parity system (N4) than the odd-parity system (N3), which may be connected to the experimentally observed larger change in the transition temperature for the even-parity systems. In addition to the bent and U-shaped conformations, we also observe some helical or twisted structures of the guest molecules that might play a role in the stability of the chiral phase. It may be mentioned here that (i) dimers having a flexible central region, for example, compounds such as the well-known CB7CB, show an inversion in the population of hairpin to extended shape of the conformers as a function of temperature [54,55], and (ii) the rigid bent nature of the main ingredient of HLC, 12OCN, is known to support chirality at a local level.

However, it would be pertinent to clarify here that, due to the inherent slow dynamics and rugged energy landscape associated with this system and the limitations of timescale practically accessible to atomistic MD simulations (a few hundreds of nanoseconds), we expect a strong nonergodicity in the conformational sampling observed in our simulations. Thus, we do not expect to be able to directly correlate or explain the experimentally observed phase behavior completely within our MD simulation study. Nonetheless, these simulation results clearly demonstrate the extent of heterogeneity in the conformational ensemble in terms of both size and shape of the host/guest molecules. We can safely conclude that the overall nature of perturbation to orientational ordering and packing of the surrounding host molecules will depend on this conformational population shift of the host molecules upon photoactivation. It is not possible to explain this phenomenon in terms of simple rigid body structural changes of the guest molecules.

We have also computed the NOP to characterize the orientational ordering among the HLC molecules upon perturbation by the guest molecules. The NOP can be defined as $\langle \frac{3}{2}\cos^2\theta - \frac{1}{2} \rangle$, where θ is the angle between the molecular long axis and the director (preferred direction of the molecules). The angular brackets indicate averaging over all molecules. Computation of the nematic director involves diagonalization of the following second-rank orientational order tensor [56,57]:

$$Q_{\alpha\beta} = \frac{1}{2N} \sum_{i=1}^{N} (3 e_{i\alpha} e_{i\beta} - \delta_{\alpha\beta}),$$

where $e_{i\alpha}$ is the αth Cartesian coordinate of the unit vector (e_i) defining the orientation of the ith molecule. The largest eigenvalue and corresponding eigenvector give the NOP and the director, respectively, for a particular configuration. The limiting values for the NOP would be 1 for an ideal nematic phase where all the molecules are perfectly aligned with the director of the system, whereas it would be 0 for an isotropic system.

As shown in Fig. 10, the change in NOP is more pronounced for the N4T-to-N4C transition than the N3T-to-N3C transition, consistent with the experimental results. Thus, the photoactivation of N4 (even parity spacer) leads to a larger perturbation in the phase behavior than N3 (odd parity spacer). This parity dependence originates from the different degrees of shift in the conformational ensemble of the guest

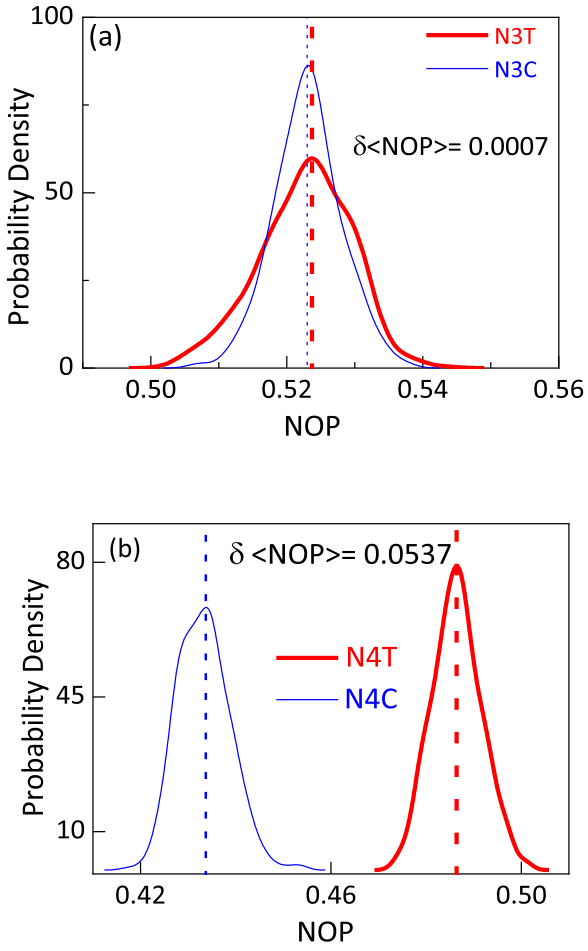

FIG. 10. Probability density (histogram) of the nematic order parameter (NOP) values calculated over the host liquid crystal (HLC) molecules in the presence of (a) N3C and N3T and (b) N4C and N4T conformations of the guest molecules.

molecules upon photoactivation, as delineated in Fig. 9. However, it must be noted that the NOP invokes a rather simplistic description of the orientational ordering of LC molecules since it captures the orientation of a single molecular axis (long) with respect to the director. However, as described above, the systems under consideration here are more complex, with two rigid arms connected by a flexible hinge. Thus, a more complex order parameter would be necessary to fully characterize the cholesteric or TGBC^* phases, which is beyond the scope of this paper. However, our present simulation work shows the richness of the systems in terms of photocontrollable conformational changes and their influence on the possible packing of molecules.

IV. SUMMARY

We have investigated both experimentally and by simulations the effect of photoisomerization on a host-guest LC system, in which the guest photoactive dopant is an azo dimer whose spacer could be of either even or odd parity. The doped mixture retains the same phase sequence as the HLC system, viz., I-N^*-TGBC^*. The photoinduced effect on the phase transition temperatures has been studied in

detail and analyzed in terms of the conformations of both host and guest molecules. Despite a small concentration (3 wt. %) of the photoactive dopant, both the I-N^* and N^*-TGBC^* transition temperatures show a remarkable odd-even effect, higher values for the even dimer mixtures than their odd counterpart; the alternation reduces with increasing n. Both the photodriven change in the transition temperatures (δT) and the transition enthalpy exhibit significant odd-even effect. To be emphasized is the feature that δT is much larger (by a factor of 8) for the N^*-TGBC^* transition than for the I-N^* one. For the I-N^* transition, the UV-on dynamic response is about an order of magnitude faster than the UV-off response, a feature that is true for all the mixtures studied. In contrast, for the N^*-TGBC^* transition, the relation depends on the length of the spacer group. Atomistic classical MD simulations have been performed to explore the conformation of the photoactive guest dopant in its equilibrium (E form) and photoactive (Z form) states. Unlike the well-known case of a monomeric azo dopant, the guest molecules employed here exist in multiple metastable states rather than in a unique conformation. The photostimulation leads to a large shift in the probability distribution of hinge angle as well as in the end-to-end distance of the molecules. The overall changes in the effective shape of the guest molecules seem to be more pronounced for the even-parity system than for the odd-parity one, perhaps resulting in a larger δT for the former, as indeed observed experimentally. The simulations also show that the change in NOP is more for the even-parity dimer.

We are extending the experimental studies to investigate the influence of photostimulation and parity aspects on the PBG features of the N^* and TGB phases. Another dimension to these studies is to have a host system which has strongly polar entities as termini along the length of the molecules. It may be pointed out that, in such systems, the photodriven odd-even effect is known to be much stronger for the I-N transition. It would certainly be interesting to see whether such a behavior is true for the N^*-TGBC^* transition as well. On the simulation front, development of a suitable order parameter to capture the N^* and TGB phases would be taken up to be able to properly characterize these phase transitions and molecular ordering associated with these processes. A full-fledged simulation work that considers the actual population of the plethora of conformers is certainly warranted to reliably compute the transition temperatures and the effect of dopants. The delicate interplay between the phototunable shape of the dopant and the required molecular packing for a particular mesophase is the essence of the observed large influence on the thermal characteristics of the medium. While a proper explanation of the differential behavior between the clearing point and the TGBC^* transition is still enigmatic, it certainly opens a vista to be explored.

ACKNOWLEDGMENTS

We thank Prof. B. L. V. Prasad, Director, CeNS, for his interest in the work and initiating the simulation work. DSSR and SKP acknowledge funding support from a SERB project (CRG/2019/001671). D.M. and S.C. thank S. N. Bose National Centre for Basic Sciences, Kolkata, for the high-performance computing facility.

The authors declare no conflict of interest.

[1] R. D. Kamien and J. V. Selinger, Order and frustration in chiral liquid crystals, J. Phys.: Condens. Matter **13**, R1 (2001).

[2] J. V. Selinger, Director deformations, geometric frustration, and modulated phases in liquid crystals, Annu. Rev. Condens. Matter Phys. **13**, 49 (2021).

[3] J. W. Goodby, A. J. Slaney, C. J. Booth, I. Nishiyama, J. D. Vuijk, P. Styring, and K. J. Toyne, Chirality and frustration in ordered fluids, Mol. Cryst. Liq. Cryst. **243**, 231 (1994).

[4] C. V. Yelamaggad, N. L. Bonde, A. S. Achalkumar, D. S. Shankar Rao, S. K. Prasad, and A. K. Prajapati, Frustrated liquid crystals: synthesis and mesomorphic behavior of unsymmetrical dimers possessing chiral and fluorescent entities, Chem. Mater. **19**, 2463 (2007).

[5] M. Kašpar, P. Bílková, A. Bubnov, V. Hamplová, V. Novotná, M. Glogarová, K. Knížek, and D. Pociecha, New chlorine-substituted liquid crystals possessing frustrated TGB_A and SmQ phases, Liq. Cryst. **35**, 641 (2008).

[6] A. Bubnov, M. Kašpar, V. Novotná, V. Hamplová, M. Glogarová, N. Kapernaum, and F. Giesselmann, Effect of lateral methoxy substitution on mesomorphic and structural properties of ferroelectric liquid crystals, Liq. Cryst. **35**, 1329 (2008).

[7] A. Poryvai, A. Bubnov, D. Pociecha, J. Svoboda, and M. Kohout, The effect of the length of terminal n-alkyl carboxylate chain on self-assembling and photosensitive properties of chiral lactic acid derivatives, J. Mol. Liq. **275**, 829 (2019).

[8] N. Tamaoki, Cholesteric liquid crystals for color information technology, Adv. Mater. **13**, 1135 (2001).

[9] V. A. Mallia and N. Tamaoki, Design of chiral dimesogens containing cholesteryl groups; formation of new molecular organizations and their application to molecular photonics, Chem. Soc. Rev. **33**, 76 (2004).

[10] P. G. de Gennes, An analogy between superconductors and smectics A, Solid State Commun. **10**, 753 (1972).

[11] R. Dhar, Twisted-grain-boundary (TGB) phases: nanostructured liquid-crystal analogue of Abrikosov vortex lattices, Phase Transitions **79**, 175 (2006).

[12] J. W. Goodby, M. A. Waugh, S. M. Stein, E. Chin, R. Pindak, and J. S. Patel, Characterization of a new helical smectic liquid crystal, Nature (London) **337**, 449 (1989).

[13] G. Srajer, R. Pindak, M. A. Waugh, J. W. Goodby, and J. S. Patel, Structural Measurements on the Liquid-Crystal Analog of the Abrikosov Phase, Phys. Rev. Lett. **64**, 1545 (1990).

[14] H. S. Kitzerow, in *Chirality in Liquid Crystals*, edited by H. S. Kitzerow and C. Bahr (Springer-Verlag, New York, 2001), pp. 296–354.

[15] W. Kuczynski and H. Stegemeyer, Twist grain boundary phases in binary mixtures, Mol. Cryst. Liq. Cryst. **260**, 377 (1995).

[16] L. Navailles, R. Pindak, P. Barois, and H. T. Nguyen, Structural Study of the Smectic-C Twist Grain Boundary Phase, Phys. Rev. Lett. **74**, 5224 (1995).

[17] For reviews and see J. W. Goodby, in *Structure and Bonding, Liquid Crystals II*, edited by D. M. P. Mingos (Springer Verlag, Berlin, 1999), pp. 83.

[18] P. A. Pramod, R. Pratibha, and N. V. Madhusudana, A three-dimensionally modulated structure in a chiral smectic-*C* liquid crystal, Curr. Sci. **73**, 761 (1997).

[19] P. A. Pramod, Y. Hatwalne, and N. V. Madhusudana, A phenomenological model for the undulating twist grain boundary-C^* phase, Liq. Cryst. **28**, 525 (2001).

[20] I. Dierking, Chiral liquid crystals: structures, phases, effects, Symmetry **6**, 444 (2014).

[21] S. Chakraborty, M. K. Das, A. Bubnov, W. Weissflog, D. Węgłowska, and R. Dabrowski, Induced frustrated twist grain boundary liquid crystalline phases in binary mixtures of achiral hockey stick-shaped and chiral rod-like materials, J. Mater. Chem. C **7**, 10530 (2019).

[22] R. Sahoo, D. S. Shankar Rao, U. S. Hiremath, C. V. Yelamaggad, P. Shinde, B. L. V. Prasad, and S. K. Prasad, Influence of gold nanorods on the structure and photonic bandgap in a twist grain boundary phase with smectic C^* blocks, J. Mol. Liq. **299**, 112117 (2020).

[23] T. Ikeda and O. Tsutsumi, Optical switching and image storage by means of azobenzene liquid-crystal films, Science **268**, 1873 (1995).

[24] H. K. Bisoyi and Q. Li, Light-driven liquid crystalline Materials: from photo-induced phase transitions and property modulations to applications, Chem. Rev. **116**, 15089 (2016).

[25] S. Krishna Prasad, G. G. Nair, and D. S. Shankar Rao, Photoinduced phase transitions, Liq. Cryst. **36**, 705 (2009).

[26] *Photoactive Functional Soft Materials: Preparation, Properties, and Applications*, edited by Q. Li (Wiley-VCH, Weinheim, 2019).

[27] *Smart Light-Responsive Materials: Azobenzene-Containing Polymers and Liquid Crystals*, edited by Y. Zhao and T. Ikeda (John Wiley & Sons, Inc., Hoboken, 2009).

[28] H. M. D. Bandara and S. C. Burdette, Photoisomerization in different classes of azobenzene, Chem. Soc. Rev. **41**, 1809 (2012).

[29] M. Mathews and N. Tamaoki, Planar chiral azobenzenes as chiroptic switches for photon mode reversible reflection color control in induced chiral nematic liquid crystals, J. Am. Chem. Soc. **130**, 11409 (2008).

[30] S. Paolonia, U. Zammit, P. Galloni, and F. Mercuria, Optically induced effects on the nematic-smecticA and smecticA-smecticC phase transitions critical behaviour in photochromic liquid crystal mixtures with different nematic range, Thermochim. Acta **695**, 178823 (2021).

[31] A. Bobrovsky, V. Shibaev, M. Cigl, V. Hamplová, D. Pociecha, and A. Bubnov, Azobenzene-containing LC polymethacrylates highly photosensitive in broad spectral range, J. Polym. Sci. Part A: Polym. Chem. **54**, 2962 (2016).

[32] A. Poryvai, A. Bubnov, and M. Kohout, Chiral photoresponsive liquid crystalline materials derived from cyanoazobenzene central core: effect of UV light illumination on mesomorphic behavior, Crystals **10**, 1161 (2020).

[33] M. Cigl, A. Bubnov, M. Kašpar, F. Hampl, V. Hamplová, O. Pacherová, and J. Svoboda, Photosensitive chiral self-assembling materials: significant effects of small lateral substituents, J. Mater. Chem. C **4**, 5326 (2016).

[34] Y. Lansac, M. Glaser, N. A. Clark, and O. D. Lavrentovich, Photocontrolled nanophase segregation in a liquid-crystal solvent, Nature (London) **398**, 54 (1999).

[35] S. Krishna prasad, G. G. Nair, and G. Hegde, Dynamic self-assembly of the liquid-crystalline smectic *A* phase, Adv. Mat. **17**, 2086 (2005).

[36] M. Y. M. Huang, A. M. Pedreira, O. G. Martins, A. M. Figueiredo Neto, and A. Jakli, Nanophase segregation of nonpolar solvents in smectic liquid crystals of bent-shape molecules, Phys. Rev. E, **66**, 031708 (2002).

[37] R. Sahoo, D. S. Shankar Rao, U. S. Hiremath, C. V. Yelamaggad, and S. K. Prasad, Impact of photoisomerization on the one-dimensional fluid and three-dimensional Abrikosov-like photonic structures of liquid crystals, J. Phys. Chem. C **124**, 13920 (2020).

[38] C. T. Imrie and G. R. Luckhurst, in *Handbook of Liquid Crystals*, 2nd ed., edited by J. W. Goodby, P. J. Collings, T. Kato, C. Tschierske, H. Gleeson, and P. Raynes, (Wiley-VCH, Weinheim, 2014), Vol. 137.

[39] C. T. Imrie, in *Liquid Crystals II. Structure and Bonding*, edited by D. M. P. Mingos (Springer, Berlin, Heidelberg, 1999), Vol. 95, pp. 149–192.

[40] C. T. Imrie and P. A. Henderson, Liquid crystal dimers and higher oligomers: between monomers and polymers, Chem. Soc. Rev. **36**, 2096 (2007).

[41] S. K. Prasad, K. L. Sandhya, G. G. Nair, U. S. Hiremath, and C. V. Yelamaggad, Spacer parity dependence of photoinduced effects in liquid-crystalline dimers, J. Appl. Phys. **92**, 838 (2002).

[42] Y. Suzuki, T. Hagiwara, I. Kawamura, N. Okamura, T. Kitazume, M. Kakimoto, Y. Imai, Y. Ouchi, H. Takezoe, and A. Fukuda, New fluorine-containing ferroelectric liquid crystal compounds showing tristable switching, Liq. Cryst. **6**, 167 (1989).

[43] L. Kovalenko, M. W. Schröder, R. Amaranatha Reddy, S. Diele, G. Pelzl, and W. Weissflog, Unusual mesomorphic behaviour of new bent-core mesogens derived from 4-cyanoresorcinol, Liq. Cryst. **32**, 857 (2005) and also prepared by Dr. C. V. Yelamaggad in our laboratory.

[44] A. E. Blatch and G. R. Luckhurst, The liquid crystal properties of symmetric and non-symmetric dimers based on the azobenzene mesogenic group, Liq. Cryst. **27**, 775 (2000) and also prepared by Dr. C. V. Yelamaggad in our laboratory.

[45] See Supplemental Material at http://link.aps.org/supplemental/10.1103/PhysRevE.106.044702 for additional figures.

[46] M. J. Abraham, T. Murtola, R. Schulz, S. Páll, J. C. Smith, B. Hess, and E. Lindahl, GROMACS: high performance molecular simulations through multi-level parallelism from laptops to supercomputers, SoftwareX **1-2**, 19 (2015).

[47] A. K. Malde, L. Zuo, M. Breeze, M. Stroet, D. Poger, P. C. Nair, C. Oostenbrink, and A. E. Mark, An automated force field topology builder (ATB) and repository: version 1.0, J. Chem. Theory Comput **7**, 4026 (2011).

[48] G. Bussi, D. Donadio, and M. Parrinello, Canonical sampling through velocity rescaling, J. Chem. Phys. **126**, 014101 (2007).

[49] M. Parrinello, Polymorphic transitions in single crystals: a new molecular dynamics method, J. Appl. Phys. **52**, 7182 (1981).

[50] W. Humphrey, A. Dalke, and K. Schulten, VMD: visual Molecular dynamics, J. Molec. Graphics **14**, 33 (1996).

[51] G. Joly, A. Anakkar, and H. T. Nguyen, Light induced shifts of ferroelectric mesophase transitions, Liq. Cryst. **26**, 1251 (1999).

[52] S. K. Prasad, P. L. Madhuri, P. Satapathy, and C. V. Yelamaggad, A soft-bent dimer composite exhibiting twist-bend nematic phase: photo-driven effects and an optical memory device, Appl. Phys. Lett. **112**, 253701 (2018).

[53] D. Chakrabarti, P. P. Jose, S. Chakrabarty, and B. Bagchi, Universal Power Law in the Orientational Relaxation in Thermotropic Liquid Crystals, Phys. Rev. Lett. **95**, 197801 (2005).

[54] S. Parthasarathi, D. S. Shankar Rao, N. B. Palakurthy, C. V. Yelamaggad, and S. K. Prasad, Effect of pressure on dielectric and frank elastic constants of a material exhibiting the twist bend nematic phase, J. Phys. Chem. B **121**, 896 (2017).

[55] D. A. Paterson, M. Gao, Y. K. Kim, A. Jamali, K. L. Finley, B. Robles-Hernández, S. Diez-Berart, J. Salud, M. R. de la Fuente, B. A. Timimi *et al.*, Understanding the twist-bend nematic phase: the characterisation of 1-(4-cyanobiphenyl-4′-yloxy)-6-(4-cyanobiphenyl-4′-yl) hexane (CB6OCB) and comparison with CB7CB, Soft Matter **12**, 6827 (2016).

[56] P. G. de Gennes and J. Prost, *The Physics of Liquid Crystals*, 2nd ed. (Clarendon Press, Oxford, 1993).

[57] S. Chakrabarty, D. Chakrabarti, and B. Bagchi, Power law relaxation and glassy dynamics in Lebwohl-Lasher model near the isotropic-nematic phase transition, Phys. Rev. E, **73**, 061706 (2006).